JACS
JOURNAL OF THE AMERICAN CHEMICAL SOCIETY
Communication
pubs.acs.org/JACS

All-Inorganic Perovskite Solar Cells

Jia Liang,[†] Caixing Wang,[†] Yanrong Wang,[†] Zhaoran Xu,[†] Zhipeng Lu,[†] Yue Ma,[†] Hongfei Zhu,[†] Yi Hu,[†] Chengcan Xiao,[†] Xu Yi,[†] Guoyin Zhu,[†] Hongling Lv,[†] Lianbo Ma,[†] Tao Chen,[†] Zuoxiu Tie,[†] Zhong Jin,*[,†] and Jie Liu*[,†,‡]

[†]Key Laboratory of Mesoscopic Chemistry of MOE and Collaborative Innovation Center of Chemistry for Life Sciences, School of Chemistry and Chemical Engineering, Nanjing University, Nanjing, Jiangsu 210093, China

[‡]Department of Chemistry, Duke University, Durham, North Carolina 27708, United States

Supporting Information

ABSTRACT: The research field on perovskite solar cells (PSCs) is seeing frequent record breaking in the power conversion efficiency (PCE). However, organic−inorganic hybrid halide perovskites and organic additives in common hole-transport materials (HTMs) exhibit poor stability against moisture and heat. Here we report the successful fabrication of all-inorganic PSCs without any labile or expensive organic components. The entire fabrication process can be operated in ambient environment without humidity control (e.g., a glovebox). Even without encapsulation, the all-inorganic PSCs present no performance degradation in humid air (90−95% relative humidity, 25 °C) for over 3 months (2640 h) and can endure extreme temperatures (100 and −22 °C). Moreover, by elimination of expensive HTMs and noble-metal electrodes, the cost was significantly reduced. The highest PCE of the first-generation all-inorganic PSCs reached 6.7%. This study opens the door for next-generation PSCs with long-term stability under harsh conditions, making practical application of PSCs a real possibility.

Since the first demonstration of the use in solar cells,[1] organic−inorganic hybrid halide perovskites have become promising candidates for efficient solar energy harvesting.[2] The power conversion efficiencies (PCEs) of perovskite solar cells (PSCs) have exhibited a meteoric rise over the past few years, and the certified highest PCE has reached 22.1% recently.[3] Despite the rapid increase in PCE associated with the evolution of new perovskite materials and fabrication techniques, the instability of PSCs remains unresolved.[4] The problem is mainly because the mostly studied hybrid perovskites, such as methylammonium lead triiodide ($MAPbI_3$) and formamidinium lead triiodide ($FAPbI_3$), have poor stability against moisture and heat. Some organic additives in commonly used hole-transport materials (HTMs), such as lithium bis(trifluoromethanesulfonyl)imide (LiTFSI) and *tert*-butylpyridine (*t*BP), are also hygroscopic and deliquescent, promoting performance degradation.[5,6] Moreover, the fabrication of hybrid PSCs still relies on precise environmental control, such as gloveboxes or dryrooms. The necessary route to improve the stability of PSCs is to explore novel perovskite materials and HTMs with high stability against humidity and heat. Besides, growing efforts are being devoted to finding cheap alternatives to replace expensive organic HTMs, such as 2,2′,7,7′-tetrakis(*N*,*N*′-di-*p*-methoxyphenylamine)-9,9′-spirobifluorene (spiro-MeOTAD) or polytriarylamine (PTAA).[7] These drawbacks, if not adequately addressed, will hinder the batch production and practical deployment of PSCs.

Since the instability of PSCs is mainly due to the decomposition of labile organic components, there are anticipated benefits to developing all-inorganic PSCs by excluding all of the organic species sensitive to the ambient environment. Following this line of thought, here we show the successful fabrication of all-inorganic PSCs without any labile or expensive organic components. The all-inorganic PSCs show remarkable stability under high-humidity conditions (90−95% relative humidity (RH), 25 °C) and extreme temperatures (100 or −22 °C) even without encapsulation, and therefore, the instability of traditional hybrid PSCs can be avoided. Unlike the hybrid PSCs, the entire fabrication process of all-inorganic PSCs can be operated in ambient atmosphere without humidity control. Also, eliminating expensive organic HTMs (~$350/g) and noble-metal electrodes (~$50/g) greatly reduces the cost, paving the way for mass production and application.

Figure 1a shows a schematic cross-sectional view of the all-inorganic PSCs. The cell consists of functional layers of fluorine-doped tin oxide (FTO)/compact TiO_2 (c-TiO_2)/mesoporous TiO_2 (m-TiO_2)/inorganic perovskite $CsPbBr_3$/carbon (see the Supporting Information (SI)). The intention behind using the inorganic perovskite $CsPbBr_3$ as the light absorber is that $CsPbBr_3$ is known to be much more stable than hybrid perovskites (e.g., $MAPbI_3$ and $FAPbI_3$) at high temperature.[8] Recent studies also showed that $CsPbBr_3$ has a high carrier mobility and mean free path.[8b] A layer of carbon was deposited on $CsPbBr_3$ to work as a bifunctional film for both effective hole extraction and collection, since it has an appropriate work function (−5.0 eV) close to that of gold (−5.1 eV).[7a,9] Moreover, the carbon electrode is very stable, processable, and cheap. Figure 1b shows the band energy levels of the FTO, TiO_2, $CsPbBr_3$, and carbon layers, revealing the smooth electron extraction from the $CsPbBr_3$ conduction band to the TiO_2 conduction band and hole extraction from the $CsPbBr_3$ valence band to the carbon electrode. Figure 1c shows the crystal structure of $CsPbBr_3$ ascribed to the cubic (*Pm*3*m*) phase, exhibiting a three-dimensional framework of corner-connected $PbBr_6$ octahedra with Cs^+ cations located between the octahedra.[8e,10] Figure 1d

Received: September 29, 2016
Published: November 26, 2016

DOI: 10.1021/jacs.6b10227
J. Am. Chem. Soc. 2016, 138, 15829−15832

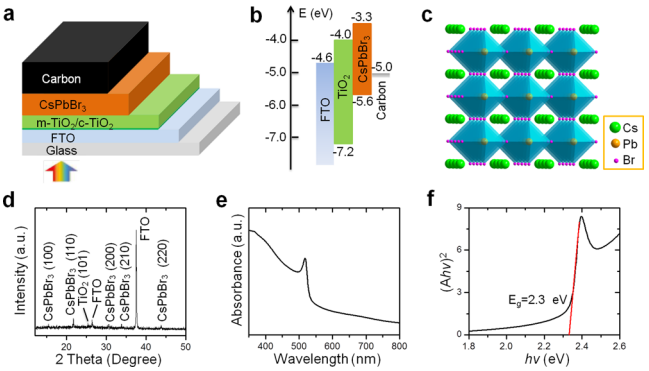

Figure 1. (a) Schematic cross-sectional view of $CsPbBr_3$/carbon-based all-inorganic PSCs with the configuration of FTO/c-TiO_2/m-TiO_2/$CsPbBr_3$/carbon. (b) Energy level diagram of the all-inorganic PSCs, showing smooth electron injection and hole extraction. (c) Crystal structure of the inorganic perovskite $CsPbBr_3$. (d) XRD pattern of the all-inorganic PSCs without the carbon layer, showing peaks generated by $CsPbBr_3$, FTO, and TiO_2. (e) Absorption spectrum and (f) corresponding $(Ahv)^2$ vs energy (hv) curve of a $CsPbBr_3$ film. The optical band gap of $CsPbBr_3$ was measured to be ~2.3 eV.

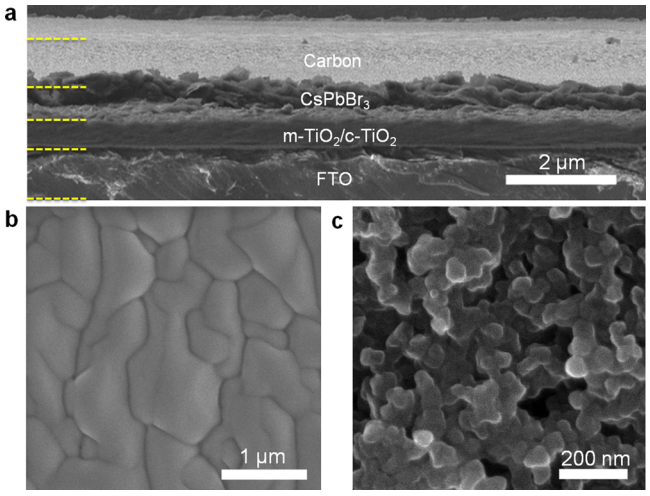

Figure 2. (a) Cross-sectional SEM image of a $CsPbBr_3$/carbon-based all-inorganic PSC. The thickness of the $CsPbBr_3$ layer between TiO_2 and the carbon electrode is ~600 nm. The carbon electrode coated by doctor blading forms a ~900 nm thick capping layer. (b) SEM image of the inorganic perovskite $CsPbBr_3$ layer. (c) SEM image of the carbon electrode that served as both the HTM and the counter electrode, showing carbon nanoparticles with average diameter of ~80 nm.

shows the X-ray diffraction (XRD) pattern of $CsPbBr_3$/carbon-based all-inorganic PSCs (without the carbon layer). In the XRD pattern, eight characteristic peaks are found, of which two are from the FTO substrate. The (101) peak of anatase TiO_2 has a relative low intensity because the c-TiO_2/m-TiO_2 layer is thin. The other five peaks are generated by the $CsPbBr_3$ layer, confirming that $CsPbBr_3$ is in the cubic perovskite phase.[8e,10] Figure 1e displays the absorbance spectrum of $CsPbBr_3$, showing that $CsPbBr_3$ absorbs light with wavelength shorter than ~540 nm. The method adopted by Tandon and Gupta was used to evaluate the optical band gap of $CsPbBr_3$.[8d] Figure 1f shows a plot of $(Ahv)^2$ versus photon energy (hv), which indicates that the band gap of $CsPbBr_3$ is ~2.3 eV. Additionally, from the valence-band XPS spectrum (Figure S1), the positions of the valence-band maximum (VBM) and conduction-band minimum (CBM) of $CsPbBr_3$ were determined (Figure 1b). Because of the high stability of all of the components in the all-inorganic PSCs and the much simpler device configuration than in traditional hybrid PSCs, the fabrication process of the all-inorganic PSCs is more feasible for large-scale production.

Figure 2a shows a scanning electron microscopy (SEM) image of the cross-sectional structure (sliced by a diamond cutter) of a $CsPbBr_3$/carbon-based all-inorganic PSC, which depicts a uniform deposition. Figure S2a,b shows plane-view SEM images of the c-TiO_2 and m-TiO_2 layers, respectively. The inorganic perovskite $CsPbBr_3$ layer has a dense and uniform surface (Figure 2b), which is beneficial for its application in PSCs. The morphology (Figure 2c) and Raman spectrum (Figure S3) of the carbon electrode that served as both the HTM and the counter electrode were also investigated. Further surface characterizations of the four functional layers (c-TiO_2, m-TiO_2, $CsPbBr_3$, and carbon) via atomic force microscopy (AFM) (Figure S4) are in accordance with the SEM characterizations. To identify the composition of the $CsPbBr_3$ layer, X-ray photoelectron spectroscopy (XPS) analysis was performed (Figure S5a). With the binding energy of the C 1s peak arising from adventitious carbon set at 284.6 eV, the attribution of other peaks was determined. Figure S5b–d presents the high-resolution XPS spectra of the Cs 3d, Pb 4f, and Br 3d regions, respectively; the binding energies and atomic ratios are listed in Table S1, confirming that the inorganic perovskite layer is $CsPbBr_3$.

Figure 3a displays the current density–voltage (J–V) plot of a $CsPbBr_3$/carbon-based all-inorganic PSC with optimized thicknesses of the m-TiO_2 and $CsPbBr_3$ layers. As control experiments, all-inorganic PSCs with other thicknesses were also fabricated, as shown in Figure S6 and Table S2. The corresponding photovoltaic parameters of the all-inorganic PSCs under the optimized conditions with an active area of 0.12 cm^2, including the short-circuit density (J_{SC}), open-circuit voltage (V_{OC}), fill factor (FF), and PCE, are summarized in the inset in Figure 3a. A PCE as high as 6.7% was obtained, which is higher than that of previous reports.[11,12] Compared with the traditional hybrid PSCs,[3a–d] the $CsPbBr_3$/carbon-based all-inorganic PSCs exhibit a lower J_{SC} but a much higher V_{OC} (Figure 1e,f). The maximum photocurrent density is ~9 mA/cm^2 because of the relatively wide band gap of $CsPbBr_3$ (2.3 eV). Intriguingly, though the band gap of $CsPbBr_3$ is unfavorable to J_{SC}, it is beneficial to V_{OC}. The V_{OC} of $CsPbBr_3$/carbon-based all-inorganic PSCs is 1.24 V, which is much higher than that of $MAPbI_3$-based hybrid PSCs.[2a,b,3a,d] In order to demonstrate the repeatability, 40 cells were fabricated and characterized (Figure 3b). The PCE histogram was distributed over a small range with an average value of 5.7%. The high reproducibility is ascribed to the homogeneous morphology and thickness of the $CsPbBr_3$ layers. It is also a result of the much simplified fabrication process due to the advantages of all-inorganic components in the devices.

The remarkable stability of $CsPbBr_3$ is an important factor that ensures the reproducibility and excellent stability of the all-inorganic PSCs. It is noteworthy that all of the fabrication steps for the all-inorganic PSCs were done in ambient air with no need of humidity or temperature control. The performance insensitivity of the all-inorganic PSCs against the environment is a major advantage for practical applications. To further demonstrate the long-term stability, the photovoltaic parameters of $CsPbBr_3$/carbon-based all-inorganic PSCs as a function of storage time in humid air (90–95% RH, 25 °C) without encapsulation were investigated (Figures 3c and S7, labeled as

DOI: 10.1021/jacs.6b10227
J. Am. Chem. Soc. 2016, 138, 15829–15832

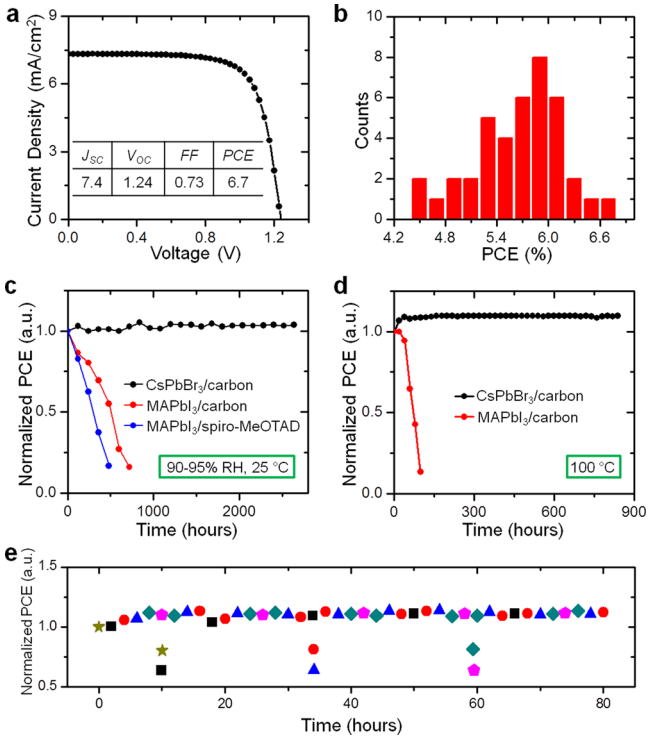

Figure 3. (a) $J-V$ plot of $CsPbBr_3$/carbon-based all-inorganic PSCs. The inset shows the corresponding photovoltaic parameters. (b) Statistical histogram of the PCEs of 40 individual $CsPbBr_3$/carbon-based all-inorganic PSCs. (c) Normalized PCEs of $CsPbBr_3$/carbon-based all-inorganic PSCs and $MAPbI_3$/carbon-based and $MAPbI_3$/spiro-MeOTAD-based hybrid PSCs as a function of storage time in humid air (90–95% RH, 25 °C) without encapsulation. (d) Normalized PCEs of $CsPbBr_3$/carbon-based all-inorganic PSCs and $MAPbI_3$/carbon-based hybrid PSCs as a function of time heated at high temperature (100 °C) in a high-humidity ambient environment (90–95% RH, 25 °C) without encapsulation. (e) Normalized PCEs of $CsPbBr_3$/carbon-based all-inorganic PSCs vs storage time during temperature cycles (between −22 and 100 °C) in a high-humidity ambient environment (90–95% RH, 25 °C) without encapsulation.

$CsPbBr_3$/carbon). As control devices, two types of reference cells based on the traditional hybrid perovskite $MAPbI_3$ with the structures of FTO/c-TiO_2/m-TiO_2/$MAPbI_3$/carbon (labeled as $MAPbI_3$/carbon) and FTO/c-TiO_2/m-TiO_2/$MAPbI_3$/spiro-MeOTAD/carbon (labeled as $MAPbI_3$/spiro-MeOTAD) were also fabricated in an Ar-filled glovebox without encapsulation. Because of the intrinsic deliquescent characteristics of $MAPbI_3$ and organic additives (LiTFSI and *t*BP) in spiro-MeOTAD, the $MAPbI_3$/spiro-MeOTAD-based hybrid PSCs show the poorest stability among the three devices. Meanwhile, the $CsPbBr_3$/carbon-based all-inorganic PSCs display significantly improved stability compared with the $MAPbI_3$/carbon-based hybrid PSCs, even though the two types of PSCs possess the same structure except for the perovskite layer. Specifically, the PCE of $CsPbBr_3$/carbon-based all-inorganic PSCs exhibited no degradation even after storage in humid air (90–95% RH, 25 °C) for more than 3 months (2640 h) without any sealing (Figure 3c). In contrast, the PCEs of the $MAPbI_3$/carbon-based and $MAPbI_3$/spiro-MeOTAD-based hybrid PSCs degraded to ∼10% of their initial values within 30 days (∼720 h) and 20 days (∼480 h), respectively, under the same conditions as a result of the great decreases in J_{SC} (Figure S7). These results indicate that the $CsPbBr_3$/carbon-based all-inorganic PSCs have far superior stability in high humidity compared with the traditional hybrid PSCs. As shown in Figure S8, the XRD patterns and photographs of a bare $CsPbBr_3$ film before and after exposure to humid air (90–95% RH, 25 °C) for 15 days show no change in XRD peaks or color, further confirming the high stability of $CsPbBr_3$ against humidity.

The stabilities of $CsPbBr_3$/carbon-based all-inorganic PSCs and $MAPbI_3$/carbon-based hybrid PSCs heated to high temperature (100 °C) in a high-humidity ambient environment (90–95% RH, 25 °C) without encapsulation were also investigated. The PCE of $CsPbBr_3$/carbon-based all-inorganic PSCs reached a stable value after 20 h and exhibited remarkable stability during a long testing period of 840 h (Figures 3d and S9). It is noteworthy that the final PCE of the $CsPbBr_3$/carbon-based all-inorganic PSCs is slightly higher than its initial value. In contrast, the PCE of $MAPbI_3$/carbon-based hybrid PSCs kept relatively stable during the first 20 h, which is attributed to the protection of the carbon electrode; however, thereafter the PCE dramatically decreased to ∼10% of its initial value within 100 h (Figures 3d and S9). This is ascribed to the rapid degradation of $MAPbI_3$. Moreover, storage in a refrigerator without encapsulation confirmed that the $CsPbBr_3$/carbon-based all-inorganic PSCs can also endure low temperature (−22 °C), as the performance showed no degradation for over 840 h (Figure S10). In real life, solar cells have to work outdoors with temperature cycles instead of constant temperature. Therefore, we also tested the stability of $CsPbBr_3$/carbon-based all-inorganic PSCs during temperature cycles between −22 and 100 °C (see the SI), as shown in Figure 3e. The results revealed that the all-inorganic PSCs exhibited no degradation during the cycles of extreme temperatures for 80 h without encapsulation, further confirming their high stability. In short, compared with the $MAPbI_3$/carbon-based hybrid PSCs, the $CsPbBr_3$/carbon-based all-inorganic PSCs show much better stability under harsh conditions without the need for any encapsulation.

Moreover, $CsPbBr_3$/carbon-based all-inorganic PSCs with large active area (1.0 cm^2) were also fabricated. Figure 4a shows

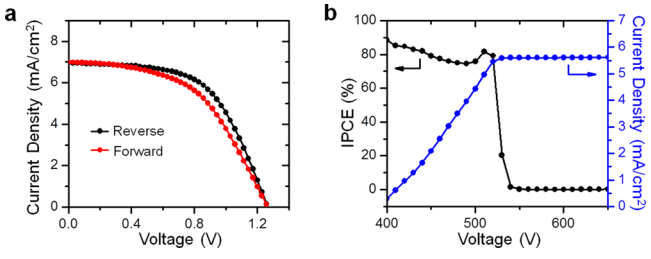

Figure 4. (a) $J-V$ plots of an all-inorganic PSC with a large active area of 1.0 cm^2 measured in the forward and reverse scanning modes. (b) IPCE spectrum and integrated current density of the PSC in (a).

the $J-V$ plots of a large-area PSC measured in the forward and reverse scanning modes, respectively. The corresponding photovoltaic parameters are summarized in Table S3. The large-area PSC exhibited a minor hysteresis between the two scanning modes and revealed a PCE of 5.0%, comparable to the average value (5.7%) of the PSCs with an active area of 0.12 cm^2. Figure 4b displays the incident photon-to-electric current conversion efficiency (IPCE) spectrum of this large-area all-inorganic PSC. The IPCE starts to increase at 540 nm, which is consistent with the UV–vis spectrum of $CsPbBr_3$ (Figure 1e), and reaches 90% at ∼400 nm. By calculation of the overlap integral of the IPCE spectrum, the integrated photocurrent density was measured to be 5.68 mA cm^{-2}, which is slightly lower

DOI: 10.1021/jacs.6b10227
J. Am. Chem. Soc. 2016, 138, 15829–15832

than the J_{SC} of 6.98 mA cm^{-2} measured from the $J-V$ curve (Figure 4a). This difference is mainly due to the fact that the IPCE in the UV region (wavelengths below 400 nm) could not be obtained because of limitations of the instrument.

Actually, not every inorganic perovskite material has such good stability. The choice of the right materials is very important. For example, the performance of cubic-phase $CsPbI_3$ with a band gap smaller than that of $CsPbBr_3$ (~1.7 eV; Figure S11) was not as outstanding as that of $CsPbBr_3$. Figure S12 and Table S4 show the $J-V$ plots and corresponding photovoltaic parameters of sealed $CsPbI_3$/carbon-based all-inorganic PSCs and after exposure to humid air (90−95% RH, 25 °C) without encapsulation for 30 and 60 s, respectively. The sealed $CsPbI_3$-based all-inorganic PSCs have a PCE of ~3.6%. However, the PCE of $CsPbI_3$/carbon-based all-inorganic PSCs exposed to humid air rapidly decreased to 1.13% after 30 s and then to 0.45% after 60 s. This is because cubic-phase $CsPbI_3$ is unstable in humid atmosphere and rapidly converts to the non-perovskite orthorhombic phase, as revealed by the color change and XRD analysis (Figure S13). Therefore, $CsPbBr_3$ proved to be a much better choice than $CsPbI_3$ for all-inorganic PSCs because of the outstanding stability. Although the PCE of $CsPbBr_3$/carbon-based all-inorganic PSCs is not quite as high because of the relatively wide band gap of $CsPbBr_3$, it is possible to reduce the band gap and further improve the PCE, e.g., by partially replacing Br^- with I^- and/or replacing Pb^{2+} with Sn^{2+},[12] to find more optimized solutions for simultaneously improving the PCE and stability. Our future work will focus on optimizing the compositions and band structures of inorganic perovskites to further improve the overall performances of all-inorganic PSCs. We expect that this study will push forward the development and practical deployment of next-generation stable and economical PSCs.

■ ASSOCIATED CONTENT

Supporting Information

The Supporting Information is available free of charge on the ACS Publications website at DOI: 10.1021/jacs.6b10227.

Experimental section and additional data (PDF)

■ AUTHOR INFORMATION

Corresponding Authors

*zhongjin@nju.edu.cn

*j.liu@duke.edu

ORCID

Zhong Jin: 0000-0001-8860-8579

Notes

The authors declare no competing financial interest.

■ ACKNOWLEDGMENTS

We thank the National Materials Genome Project (2016YFB0700600), the National Basic Research Program (2015CB659300), the National Natural Science Foundation of China (21403105, 21573108), the China Postdoctoral Science Foundation (2015M580413, 2015M581769, 2015M581775), the Natural Science Foundation for Young Scholars of Jiangsu Province (BK20160647, BK20150571, BK20150583), the Fundamental Research Funds for the Central Universities, and the Priority Academic Program Development of Jiangsu Higher Education Institutions for support.

■ REFERENCES

(1) Kojima, A.; Teshima, K.; Shirai, Y.; Miyasaka, T. *J. Am. Chem. Soc.* **2009**, *131*, 6050.

(2) (a) Liu, M.; Johnston, M. B.; Snaith, H. J. *Nature* **2013**, *501*, 395. (b) Burschka, J.; Pellet, N.; Moon, S.; Humphry-Baker, R.; Gao, P.; Nazeeruddin, M.; Gratzel, M. *Nature* **2013**, *499*, 316. (c) Kim, H.-S.; Lee, C.-R.; Im, J.-H.; Lee, K.-B.; Moehl, T.; Marchioro, A.; Moon, S.-J.; Humphry-Baker, R.; Yum, J.-H.; Moser, J. E.; Grätzel, M.; Park, N.-G. *Sci. Rep.* **2012**, *2*, 591. (d) Xing, G.; Mathews, N.; Sun, S.; Lim, S.; Lam, Y.; Grätzel, M.; Mhaisalkar, S.; Sum, T. *Science* **2013**, *342*, 344. (e) Stranks, S.; Eperon, G.; Grancini, G.; Menelaou, C.; Alcocer, M.; Leijtens, T.; Herz, L.; Petrozza, A.; Snaith, H. *Science* **2013**, *342*, 341. (f) Shi, D.; Adinolfi, V.; Comin, R.; Yuan, M.; Alarousu, E.; Buin, A.; Chen, Y.; Hoogland, S.; Rothenberger, A.; Katsiev, K.; Losovyj, Y.; Zhang, X.; Dowben, P.; Mohammed, O.; Sargent, E.; Bakr, O. *Science* **2015**, *347*, 519. (g) Dong, Q.; Fang, Y.; Shao, Y.; Mulligan, P.; Qiu, J.; Cao, L.; Huang, J. *Science* **2015**, *347*, 967.

(3) (a) Zhou, H.; Chen, Q.; Li, G.; Luo, S.; Song, T.; Duan, H.; Hong, Z.; You, J.; Liu, Y.; Yang, Y. *Science* **2014**, *345*, 542. (b) Jeon, N.; Noh, J.; Yang, W.; Kim, Y.; Ryu, S.; Seo, J.; Seok, S. *Nature* **2015**, *517*, 476. (c) Yang, W.; Noh, J.; Jeon, N.; Kim, Y.; Ryu, S.; Seo, J.; Seok, S. *Science* **2015**, *348*, 1234. (d) Chen, W.; Wu, Y.; Yue, Y.; Liu, J.; Zhang, W.; Yang, X.; Chen, H.; Bi, E.; Ashraful, I.; Gratzel, M.; Han, L. *Science* **2015**, *350*, 944. (e) http://www.nrel.gov/pv/assets/images/efficiency_chart.jpg (accessed Sept 29, 2016).

(4) (a) You, J.; Meng, L.; Song, T.; Guo, T.; Yang, Y.; Chang, W.; Hong, Z.; Chen, H.; Zhou, H.; Chen, Q.; Liu, Y.; De Marco, N.; Yang, Y. *Nat. Nanotechnol.* **2016**, *11*, 75. (b) Tai, Q.; You, P.; Sang, H.; Liu, Z.; Hu, C.; Chan, H.; Yan, F. *Nat. Commun.* **2016**, *7*, 11105. (c) Kaltenbrunner, M.; Adam, G.; Glowacki, E.; Drack, M.; Schwodiauer, R.; Leonat, L.; Apaydin, D.; Groiss, H.; Scharber, M.; White, M.; Sariciftci, N.; Bauer, S. *Nat. Mater.* **2015**, *14*, 1032. (d) Tsai, H.; Nie, W.; Blancon, J.; Stoumpos, C.; Asadpour, R.; Harutyunyan, B.; Neukirch, A.; Verduzco, R.; Crochet, J.; Tretiak, S.; Pedesseau, L.; Even, J.; Alam, M.; Gupta, G.; Lou, J.; Ajayan, P.; Bedzyk, M.; Kanatzidis, M.; Mohite, A. D. *Nature* **2016**, *536*, 312. (e) Li, X.; Dar, M. I.; Yi, C.; Luo, J.; Tschumi, M.; Zakeeruddin, S.; Nazeeruddin, M.; Han, H.; Gratzel, M. *Nat. Chem.* **2015**, *7*, 703. (f) Leijtens, T.; Eperon, G.; Noel, N.; Habisreutinger, S.; Petrozza, A.; Snaith, H. *Adv. Energy Mater.* **2015**, *5*, 1500963. (g) Manser, J.; Saidaminov, M.; Christians, J.; Bakr, O.; Kamat, P. *Acc. Chem. Res.* **2016**, *49*, 330.

(5) Liu, J.; Wu, Y.; Qin, C.; Yang, X.; Yasuda, T.; Islam, A.; Zhang, K.; Peng, W.; Chen, W.; Han, L. *Energy Environ. Sci.* **2014**, *7*, 2963.

(6) Kazim, S.; Ramos, F.; Gao, P.; Nazeeruddin, M.; Gratzel, M.; Ahmad, S. *Energy Environ. Sci.* **2015**, *8*, 1816.

(7) (a) Mei, A.; Li, X.; Liu, L.; Ku, Z.; Liu, T.; Rong, Y.; Xu, M.; Hu, M.; Chen, J.; Yang, Y.; Gratzel, M.; Han, L. *Science* **2014**, *345*, 295. (b) Christians, J.; Fung, R.; Kamat, P. *J. Am. Chem. Soc.* **2014**, *136*, 758. (c) Wang, K.; Jeng, J.; Shen, P.; Chang, Y.; Diau, E.; Tsai, C.; Chao, T.; Hsu, H.; Lin, P.; Chen, P.; Guo, T.; Wen, T. *Sci. Rep.* **2014**, *4*, 4756.

(8) (a) Chung, I.; Song, J.; Im, J.; Androulakis, J.; Malliakas, C.; Li, H.; Freeman, A.; Kenney, J.; Kanatzidis, M. *J. Am. Chem. Soc.* **2012**, *134*, 8579. (b) Yettapu, G.; Talukdar, D.; Sarkar, S.; Swarnkar, A.; Nag, A.; Ghosh, P.; Mandal, P. *Nano Lett.* **2016**, *16*, 4838. (c) Kulbak, M.; Cahen, D.; Hodes, G. *J. Phys. Chem. Lett.* **2015**, *6*, 2452. (d) Chung, I.; Lee, B.; He, J.; Chang, R.; Kanatzidis, M. *Nature* **2012**, *485*, 486. (e) Akkerman, Q.; Motti, S.; Srimath Kandada, A. R.; Mosconi, E.; D'Innocenzo, V.; Bertoni, G.; Marras, S.; Kamino, B.; Miranda, L.; De Angelis, F.; Petrozza, A.; Prato, M.; Manna, L. *J. Am. Chem. Soc.* **2016**, *138*, 1010.

(9) Etgar, L.; Gao, P.; Xue, Z.; Peng, Q.; Chandiran, A.; Liu, B.; Nazeeruddin, M.; Gratzel, M. *J. Am. Chem. Soc.* **2012**, *134*, 17396.

(10) Akkerman, Q.; D'Innocenzo, V.; Accornero, S.; Scarpellini, A.; Petrozza, A.; Prato, M.; Manna, L. *J. Am. Chem. Soc.* **2015**, *137*, 10276.

(11) Kulbak, M.; Gupta, S.; Kedem, N.; Levine, I.; Bendikov, T.; Hodes, G.; Cahen, D. *J. Phys. Chem. Lett.* **2016**, *7*, 167.

(12) Ma, Q.; Huang, S.; Wen, X.; Green, M.; Ho-Baillie, A. *Adv. Energy Mater.* **2016**, *6*, 1502202.

DOI: 10.1021/jacs.6b10227
J. Am. Chem. Soc. 2016, 138, 15829−15832